Observation of Asymmetric Transport in Structures with Active Nonlinearities

N. Bender, S. Factor, J. D. Bodyfelt, H. Ramezani, D. N. Christodoulides, F. M. Ellis, and T. Kottos

Phys. Rev. Lett. **110**, 234101 — Published 4 June 2013

DOI: 10.1103/PhysRevLett.110.234101

Observation of Asymmetric Transport in Structures with $\mathcal{PT}$-symmetric Nonlinearities

N. Bender[1], S. Factor[1], J. D. Bodyfelt[1,2], H. Ramezani[1], D. N. Christodoulides[3], F. M. Ellis[1], T. Kottos[1]
[1]*Department of Physics, Wesleyan University, Middletown, CT-06459, USA*
[2]*Electroscience Laboratory, Ohio State University, Columbus, OH 43212 and*
[3]*College of Optics & Photonics-CREOL, University of Central Florida, Orlando, Florida 32816, USA*
(Dated: April 24, 2013)

A mechanism for asymmetric transport which is based on parity-time ($\mathcal{PT}$) symmetric nonlinearities is presented. We show that in contrast to the case of conservative nonlinearities, an increase of the complementary conductance strength leads to a simultaneous increase of asymmetry and transmittance intensity. We experimentally demonstrate the phenomenon using a pair of coupled van der Pol oscillators as a reference system, each with complementary anharmonic gain and loss conductances, connected to transmission lines. An equivalent optical set-up is also proposed.

PACS numbers: 05.45.-a, 42.25.Bs, 11.30.Er

Directed transport is at the heart of many fundamental problems in physics. Furthermore it is of importance to engineering where the challenge is to design on-chip integrated devices that control energy and/or mass flows in different spatial directions. Along these lines, the creation of novel classes of integrated photonic, electronic, acoustic or thermal diodes is of great interest and constitute the basic building blocks for a variety of transport-based devices such as rectifiers, pumps, molecular switches and transistors.

The idea was originally implemented in the electronics framework, with the construction of electrical diodes that were able to rectify the current flux. This significant revolution motivated researchers to investigate the possibility of implementing this idea of "diode action" to other areas. For example, a proposal for the creation of a thermal diode, capable of transmitting heat asymmetrically between two temperature sources, was suggested in Ref. [1]. Another domain of application was the propagation of acoustic pulses in granular systems [2].

A related issue concerns the possibility of devising an optical diode which transmits light differently along opposite propagation directions. Currently, such unidirectional elements rely almost exclusively on the Faraday effect, where external magnetic fields are used to break space-time symmetry. Generally this requires materials with appreciable Verdet constants and/or large size nonreciprocal devices – typically not compatible with on-chip integration schemes or light-emitting wafers [3]. To address these problems, alternative proposals for the creation of optical diodes have been suggested recently. Examples include optical diodes based on second harmonic generation in asymmetric waveguides [4], nonlinear photonic band-gap materials [5], photonic quasi-crystals and molecules [6], or asymmetric nonlinear structures [7]. Most of these schemes, however, suffer from serious drawbacks making them unsuitable for commercial or small-scale applications. Relatively large physical sizes are often needed while absorption or direct reflection dramatically affects the functionality leading to an inadequate balance between figures of merit and optical intensities. In other cases, cumbersome structural designs are necessary to provide structural asymmetry, or the transmitted signal has different characteristics than the incident one.

In this Letter we, experimentally and theoretically, demonstrate a mechanism for asymmetric transport exploiting the co-existence of active elements with distinctive features of nonlinear dynamical systems, such as amplitude-dependent resonances. As a reference model we will use coupled nonlinear electronic Van der Pol (VDP) oscillators [8] with anharmonic parts consisting of a complementary amplifier (gain) and a dissipative conductor (loss) combined to preserve parity-time ($\mathcal{PT}$) symmetry (see Fig 1a). $\mathcal{PT}$-symmetric structures were inspired by quantum field theories [9]; their technological importance was first recognized in the framework of optics [10], where several intriguing features were found [10–21]. For example, the theoretical proposal of Refs. [20, 21] suggested using nonlinearities to induce asymmetric transport. Very recently the idea of creating $\mathcal{PT}$-symmetric devices within the electronics framework was proposed and experimentally demonstrated in Ref. [22]. $\mathcal{PT}$-electronics provides a platform for detailed scrutiny of many new concepts within a framework of easily accessible experimental configurations [22–24]. Despite all this activity, the majority of $\mathcal{PT}$-symmetric Hamiltonians introduced in quantum field theory, optics, and electronics have been restricted to conservative anharmonic constituents (if any) with the matched gain and loss exclusively linear (see however the theoretical works [25–27]).

Below we exploit the simplicity of the electronic circuitry framework in order to demonstrate with experiment, simulations, and theory, asymmetric transport from $\mathcal{PT}$-symmetric structures that belong to a relatively unexplored class of nonlinear systems whose anharmonic parts includes the mutually matched gain and loss. We remark, however, that our proposal can be implemented in optics (see Fig. 1b) by employing concatenated semiconductor optical amplifier and semiconductor-doped two-photon absorber microcavities.

An ideal VDP oscillator has a linear anti-damping

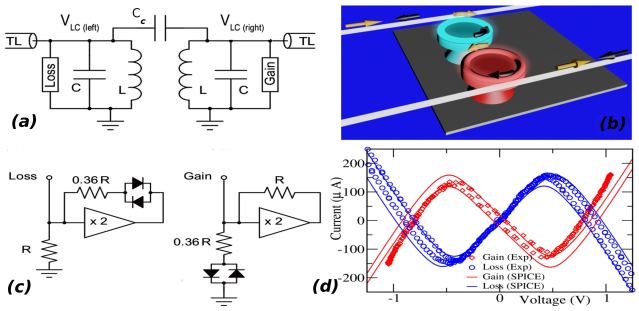

FIG. 1: (Color Online) (a) A non-linear $\mathcal{PT}$-symmetric electronic dimer; (b) The equivalent optics set-up consisting of two non-linear microcavities, one with gain and another with loss; (c) Gain and loss circuits of the van der Pol $\mathcal{PT}$-symmetric dimer; (d) Experimental I-V response (circles) for the gain (red) and loss (blue) elements along with the corresponding NGSPICE simulations (solid), taken at a frequency of $30kHz$, typical of the active range of the VDP dimer.

at low amplitudes which is subsequently overtaken by a cubic dissipation at high amplitudes. In electronics this is an LC oscillator in parallel with a voltage dependent conductance characterized by the I-V curve $I(V) = -V/R + bV^3$ where b is a nonlinear strength. A negative impedance converter (NIC) (right circuit of Fig. 1c) generates a $-1/R$ term, and we approximate the cubic turn-around with parallel back-to-back diodes moderated by a resistor. The time-reversed conductance is constructed with the resistor R and the diode combination interchanged (left circuit of Fig. 1c). The resulting "gain" and "loss" nonlinear conductances refer to their low amplitude character. The respective nonlinear I-V curves of the gain and loss elements are shown in Fig. 1d. The slight re-trace errors that we observe will be discussed latter in connection with the simulations. The $0.36R$ in series with the diodes optimizes the experimental /simulation match to the cubic nonlinearity used in the theory. It is important to note that only the parameter R is used to set the gain/loss parameter $\gamma = R^{-1}\sqrt{L/C}$, while the diode turn-on characteristics are fixed. When comparisons are made to theoretical models, the voltage scaling will consequently depend on γ.

The schematic of the complete dimer circuit is shown in the circuit of Fig. 1a. The coupled LC heart of the circuit is identical to that used in a previous work [22] with the gain and loss elements modified by the I-V nonlinearity. The complementary VDP oscillators are capacitively coupled by C_c.

Transmission lines (TL) with impedance Z_0 are attached to the left (loss) and the right (gain) LC nodes of the dimer to complete the scattering system used to perform our transport measurements. Experimentally, these take the form of resistances $R_0 = Z_0$ in series with independent voltage sources, here HP3325A synthesizers, on the right and left sides. The incoming and outgoing traveling wave components associated with a particular TL are deduced from the complex voltages on both ends of R_0, as sampled by a Tektronix DPO2014 oscilloscope. For example, on the left (lossy) side, with V_{LC} the voltage amplitude on the left dimer circuit node, and V_0 the voltage amplitude on the synthesizer side of the coupling resistor R_0, the incident wave on the dimer has a voltage amplitude $V_L^+ = V_0/2$ and the outgoing wave has a voltage amplitude $V_L^- = V_{LC} - V_0/2$. An equivalent relation for V_R^+ and V_R^- holds for the right TL terminal with the $\pm$ superscripts interchanged, since they refer to right or left wave traveling direction regardless of the terminal orientation.

The scattering measurements are performed for fixed incoming wave amplitude set by V_0 of the signal generator on either the left or the right side with the other side set to zero. The generator frequency is stepped (up or down), and the three relevant waveforms, V_0 and V_{LC} on the left and right are simultaneously captured (the V_0 channel on the transmitted side is zero). Harmonic components of each wave constituent can be independently analyzed for magnitude and relative phase. Instrumentation noise and sample time determine the accuracy of this analysis, which was found to be $< 1\%$.

Circuit behavior was numerically modeled by the NGSPICE simulator [28]. In Fig.1, circuit analysis was done in the time-domain for the individual gain or loss elements. Using initial DC operating conditions, an oscillating voltage source drives the circuit through a transient regime into steady-state operation, at which point the voltages and currents are recorded. Using SPICE modeling we were able to confirm that the slight re-trace errors that are observed in the IV experimental curves shown in Fig. 1 result from slew effects in the LM356 op-amps serving in the NICs.

The transmittances $T(\nu)$ versus the driving frequency ν in Fig. 2 are similarly obtained with R_0 in series with a drive V_0 standing in for the TL. The steady-state time-domain simulations for the $\mathcal{PT}$-symmetric dimer in the scattering configuration are now obtained. Fourier analysis is used to extract the relevant frequency-dependent voltages and currents, which are then used to calculate the scattering parameters. As a check of the accuracy of our numerical approach, we have also extracted the transmittance using a nonlinear harmonic balance circuit analysis [29]. We have confirmed that the results are identical, within numerical accuracy, to the ones obtained from the time-domain analysis. In Fig. 2 we also report the experimental left and right transmittances for the $\mathcal{PT}$-symmetric VDP dimer. The overall shape of the measured transmittances reasonably match the numerical simulations. The deviations are associated with a small parasitic inductive coupling, which we have experimentally verified to have a dominant influence on the lower mode (note the frequency asymmetry in the experimental curve of transmitance in Fig. 2). The effects of small influences are magnified by the resonant character of the physically significant regions.

A striking feature of the results of Fig. 2 is the fact that

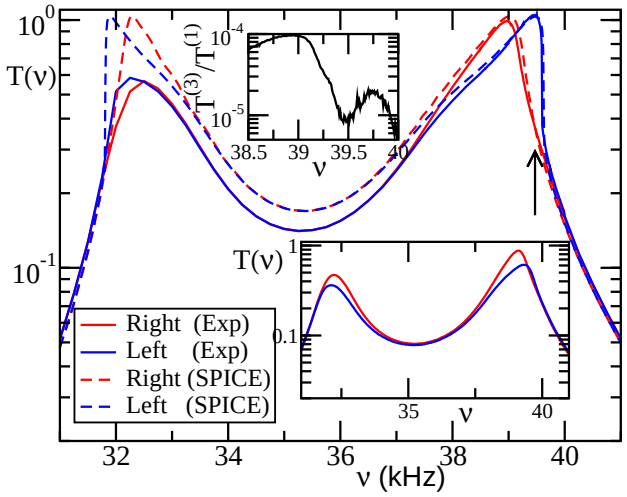

FIG. 2: (Color online) Experimental data of transmittances T_L and T_R for a left (solid blue line) and right (solid red line) incident waves. The results of the numerical simulations with SPICE for $T_L(T_R)$ transmittances are shown as dashed blue (red) lines. The arrow at 39.5 kHz shows the position of maximal asymmetry. Upper inset: The ratio between the experimental transmittances associated with the third harmonic $T^{(3)}$ and the fundamental frequency $T^{(1)}$. Here, $\eta = 0.031$ and $\gamma = 0.15$. Lower inset: Experimental $T(\nu)$ for the same η but smaller gain/loss parameter $\gamma = 0.11$. Note that as γ decreases, the asymmetry and the transmitted intensity are both reduced.

the transmittance from left to right $T_L(\nu)$ differs from the transmittance from right to left $T_R(\nu)$, i.e. $T_L \neq T_R$. The phenomenon is most pronounced in the regions of the resonances distorted by the nonlinearity, indicated by the arrow at 39.5 kHz, and is the main result of this paper. This asymmetry is forbidden by the reciprocity theorem in the case of linear, time-reversal symmetric systems [30]. In fact, it is not present even in the case of linear $\mathcal{PT}$-symmetric structures [23]. At the same time, a conservative nonlinear medium by itself cannot generate such transport asymmetries. Furthermore, we find that increasing the gain/loss parameter γ which is responsible for the asymmetric transport, maintains or even enhances the transmitted intensities while it leaves unaffected the resonance position (compare the lower inset of Fig. 2 with the main panel). This has to be contrasted with other proposals of asymmetric transport which are based on conservative non-linear schemes (see for example Ref. [7]), where increase of asymmetry leads to reduced transmittances.

We have also confirmed via direct measurements that the observed asymmetric transport is not related to the generation of higher harmonics in the output signal. In the upper inset of Fig. 2 we report the ratio $T^{(3)}/T^{(1)}$ between experimental transmittances of the third harmonic to the fundamental. Even harmonics are absent in the transmission spectra due to the nature of VDP anharmonicity, while for higher harmonics $T^{(n>3)}$ the experimental values of $T^{(n)}/T^{(1)}$ are below the noise level of our measurements. These results are also supported by the SPICE simulations (not shown). We emphasize that our definition of a rectifying structure is related to the fact that the transmitted power at fixed incident amplitude and at the *same frequency* should be sensibly different in the two opposite propagation directions. The role of the nonlinearity is confined primarily to currents internal to the dimer, while their harmonic contribution to the TL signals is suppressed by the resonant nature of the LC elements.

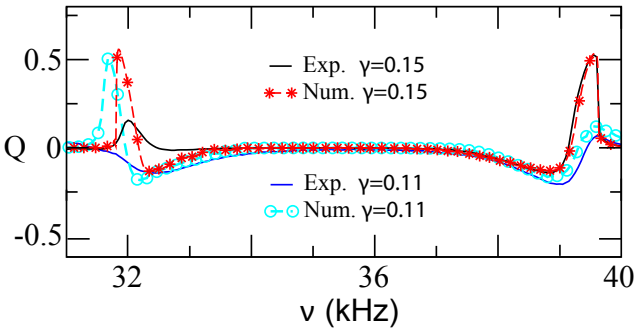

FIG. 3: (Color online) Experimental (solid lines) and SPICE (symbols) results for the rectification factor Q Eq. (1) for the coupled $\mathcal{PT}$-symmetric VDP dimer of Fig. 1 with two different γ values and $\eta = 0.03$. The Q-factor increases with the conductance strength parameter γ.

Since the phenomenon is nonlinear, the asymmetry depends on both frequency and amplitude. To quantify its efficiency, we report the rectification factor

$$Q = \frac{T_L - T_R}{T_L + T_R} \tag{1}$$

which is zero for symmetric transport and approaches ± 1 for maximal asymmetry. Some representative experimental rectification factors Q for two different values of γ are shown in Fig. 3 together with the SPICE simulations. The measurements and the simulations compare nicely with one another. Note that increasing γ broadens the regions in which $|Q|$ is relatively large.

As discussed above the asymmetry between left and right transmittances does not rely on the presence of higher harmonics but rather on the interplay of nonlinear elements with the $\mathcal{PT}$-symmetry. To unveil the importance of these features we have developed a theoretical understanding of asymmetric transport by restricting our analysis to the basic harmonic. Application of the first and second Kirchoff's laws at the TL-dimer contacts allow us to find the current/voltage wave amplitudes I, V at the left (L) and right (R) contact. We get

$$\eta \frac{d\mathcal{I}_L}{d\tau} = \gamma(1-\mathcal{V}_L^2)\frac{d\mathcal{V}_L}{d\tau} + \mathcal{V}_L + (1+c)\frac{d^2\mathcal{V}_L}{d\tau^2} - c\frac{d^2\mathcal{V}_R}{d\tau^2}, \tag{2}$$
$$\eta \frac{d\mathcal{I}_R}{d\tau} = \gamma(1-\mathcal{V}_R^2)\frac{d\mathcal{V}_R}{d\tau} - \mathcal{V}_R - (1+c)\frac{d^2\mathcal{V}_R}{d\tau^2} + c\frac{d^2\mathcal{V}_L}{d\tau^2}$$

where the dimensionless current/voltage amplitudes $\mathcal{I}, \mathcal{V}$ at the lead-dimer contacts are defined as $I_{L/R} = \mathcal{I}_{L/R}/(Z_0\sqrt{3bR})$, $V = \mathcal{V}_{L/R}/\sqrt{3bR}$. The dimensionless time is $\tau = t/\sqrt{LC}$ and $\eta = \sqrt{L/C}/Z_0$ is the dimensionless TL conductance, while we have also introduced the dimensionless capacitance $c = C_c/C$, a measure of the intra-dimer coupling. Note that Eqs. (2) are invariant under a joint $\mathcal{P}$ (i.e. $L \leftrightarrow R$) and $\mathcal{T}$ (i.e. $t \leftrightarrow -t$) operation.

At any point along a TL, the current and voltage determine the amplitudes of the right and left traveling wave components. The forward $\mathcal{V}^+_{L/R}$ and backward $\mathcal{V}^-_{L/R}$ wave amplitudes, and the voltage $\mathcal{V}_{L/R}$ and current $\mathcal{I}_{L/R}$ at the TL-dimer contacts satisfy the continuity relation

$$\begin{aligned} \mathcal{V}_{L/R} &= \left(\mathcal{V}^+_{L/R} + \mathcal{V}^-_{L/R}\right) e^{-i\omega\tau} + cc; \\ \mathcal{I}_{L/R} &= \left(\mathcal{V}^+_{L/R} - \mathcal{V}^-_{L/R}\right) e^{-i\omega\tau} + cc. \end{aligned} \tag{3}$$

Note that Eqs. (2) contains nonlinear terms on the r.h.s. which are responsible for harmonic generation. However, as suggested by the experimental data, we can neglect these higher harmonics and thus restrict our analytic study to the fundamental. Keeping this in mind when substituting Eqs. (3) into Eqs. (2), we get

$$\begin{aligned} (-1)^s i\omega\eta(-\mathcal{V}^+_{L/R} + \mathcal{V}^-_{L/R}) &= \left[1 - \omega^2(1+c) + i(-1)^{s+1}\omega\gamma(1 - |\mathcal{V}^+_{L/R} + \mathcal{V}^-_{L/R}|^2)\right](\mathcal{V}^+_{L/R} + \mathcal{V}^-_{L/R}) + c\omega^2\mathcal{V}^{+/-}_{R/L} \\ i\omega\eta(\mathcal{V}^{+/-}_{R/L}) &= \left[(-1)^s i\omega\gamma(1 - |\mathcal{V}^{+/-}_{R/L}|^2) - (1+c)\omega^2 + 1\right]\mathcal{V}^{+/-}_{R/L} + c\omega^2(\mathcal{V}^+_{L/R} + \mathcal{V}^-_{L/R}) \end{aligned} \tag{4}$$

where we used the compact notation $\mathcal{V}^{+/-}_{R/L}$ for $\mathcal{V}^+_R$ and $\mathcal{V}^-_L$. The exponent s above takes the values $s = 0, 1$ for L, R current amplitudes respectively.

We solve Eqs. (4) with the use of backward transfer map [31]. The latter uses the output amplitude $\mathcal{V}_{\rm out} = \mathcal{V}^+_R(\mathcal{V}^-_L)$ as an initial condition together with the boundary conditions $\mathcal{V}^-_R = 0$ ($\mathcal{V}^+_L = 0$) for a left (right) incoming wave. Iterating backwards, we calculate the corresponding incident $\mathcal{V}_{\rm in} = \mathcal{V}^+_L$ ($\mathcal{V}^-_R$) and reflected $\mathcal{V}_{\rm refl} = \mathcal{V}^-_L$ ($\mathcal{V}^+_R$) amplitudes for a left (right) incident wave. Representative $(|\mathcal{V}_{\rm in}|^2, |\mathcal{V}_{\rm out}|^2)$ curves are shown in Fig. 4. We have confirmed by numerical integration of the equations of motion (Eqs. 2) into steady state, that the backward transfer map is accurate to within 1% below an output amplitude of ~ 1.15. We emphasize that precise agreement between theory and the experimental data is sensitive to the exact form used for the nonlinearity, cubic for the theoretical vs. that shown in Fig. 1 for the experiment, exacerbated by the predominance of the effect in the vicinity of resonance. The associated transmittances are defined as $T \equiv |\mathcal{V}_{\rm out}/\mathcal{V}_{\rm in}|^2$. Straightforward algebra gives:

$$T_L = \Big| \frac{2\omega\eta c}{\eta\alpha + \alpha\big(\gamma(1 - |\frac{\alpha\mathcal{V}_{\rm out}}{c\omega}|^2) + \frac{i}{\omega} - i\omega(1+c)\big) + (c\omega)^2} \Big|^2, \tag{5}$$

where $\alpha = \big(\eta - \gamma(1 - |\mathcal{V}_{out}|^2) + \frac{i}{\omega} - i\omega(1+c)\big)$. The transmittance T_R for a right incident wave is given by the same expression as Eq. (5) with the substitution of $\gamma \to -\gamma$ i.e. $T_R(\gamma) = T_L(-\gamma) \neq T_L(\gamma)$. Obviously for $\gamma = 0$ (linear passive dimer) we have $T_L = T_R$. We have also check (inset of Fig. 4) that a non-linear dimer with uniform distributed gain or loss in both sites, does not result in asymmetric transport. We conclude therefore that the origin of asymmetry transport is due to the fact that nonlinear resonances are detuned differently for left (i.e. insert from lossy site) and right (i.e. insert from gain site) incident waves, as seen from Eq. (5).

Conclusions - Using coupled $\mathcal{PT}$-symmetric nonlinear VDP oscillators, we have demonstrated experimentally and theoretically an asymmetric wave transport mechanism which is based on the co-existence of nonlinearity and $\mathcal{PT}$ -symmetry. Contrary to other non-linear isolation schemes, we find that the transmitted signal remains relatively unpolluted by higher harmonics. At the same time the $\mathcal{PT}$-symmetry guarantees a high asymmetric ratio without compromising the intensity of the transmitted signal. Finally it will be interesting to use our simple anharmonic $\mathcal{PT}$-symmetric electronic framework in order to experimentally investigate other novel phenomena like $\mathcal{PT}$-solitons, nonlinear Fano resonances, perfect-transmission [25, 26].

Acknowledgments – This research was supported by an AFOSR grant No. FA 9550-10-1-0433, and by an NSF ECCS-1128571 grant. NB&SF acknowledge support from Wesleyan Faculty/Student Internship grants.

[1] M. Terraneo, M. Peyrard, G. Casati, Phys. Rev. Lett. **88**, 094302 (2002); D. Segal, A. Nitzan, ibid. **94**, 034301 (2005); C. W. Chang *et al.*, Science **314** 1121 (2006).
[2] V. F. Nesterenko *et al.*, Phys. Rev. Lett. **95**, 158702

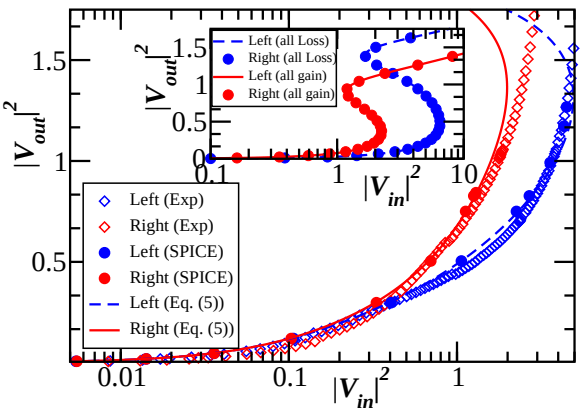

FIG. 4: (Color online) Transmission curves $|\mathcal{V}_{\rm out/in}|^2$ for a nonlinear $\mathcal{PT}$-symmetric VDP dimer with $\gamma = 0.14$, $\eta = 0.03$, $\omega = 0.98$, and $c = 0.27$. The results from Eq. (5) are compared together with the experimental data and the SPICE simulations. An asymmetry bewteen a left (indicated as Left in the figure) and right (indicated as Right in the figure) incident wave is evident. Inset: For a dimer with both sites having the same amount of loss (blue dashed line and blue circles) or gain (red line and red circles) the transmission curves are the same for left or right incident waves. In the inset we have used the theoretical expression Eq. (5).

(2005).
[3] B. E. A. Saleh and M. C. Teich, *Fundamentals of Photonics* (Wiley, New York, 1991).
[4] K. Gallo, G. Assanto, JOSA B **16**, 267 (1999); K. Gallo *et al.*, Appl. Phys. Lett. **79**, 314 (2001).
[5] M. Scalora *et al.*, J. Appl. Phys. **76**, 2023 (1994).
[6] F. Biancalana, J. of Appl. Phys. **104**, 093113 (2008).
[7] S. Lepri, G. Casati, Phys. Rev. Lett. **106**, 164101 (2011)
[8] B. van der Pol, The London, Edinburgh and Dublin Phil. Mag. & J. of Sci., **2**, 978 (1927); I. Pastor-Diaz, A. Lopez-Fraguas, Phys. Rev. E **52**, 1480 (1995).
[9] C. M. Bender and S. Boettcher, Phys. Rev. Lett. **80**, 5243 (1998); C. M. Bender, Rep. Prog. Phys. **70**, 947 (2007).
[10] K. G. Makris *et al.*, Phys. Rev. Lett. **100**, 103904 (2008); Z. H. Musslimani *et al.*, ibid. **100**, 030402 (2008); A Ruschhaupt, F Delgado and J G Muga, J. Phys. A **38**, L171 (2005).
[11] C. E. Rüter *et al.*, Nat. Phys. **6**, 192 (2010).
[12] A. Guo, *et al.*, Phys. Rev. Lett. **103**, 093902 (2009)
[13] T. Kottos, Nature Physics **6**, 166 (2010).
[14] M. C. Zheng *et al.*, Phys. Rev. A **82**, 010103 (2010).
[15] M. Liertzer *et al.*, Phys. Rev. Lett. **108**, 173901 (2012)
[16] A. Mostafazadeh, Phys. Rev. Lett. **102**, 220402 (2009).
[17] S. Longhi, Phys. Rev. A **82**, 031801 (2010); Y. D. Chong, L. Ge, A. D. Stone, Phys. Rev. Lett. **106**, 093902 (2011).
[18] O. Bendix, *et al.*, Phys. Rev. Lett. **103**, 030402 (2009); C. T. West, T. Kottos, T. Prosen, *ibid.* **104**, 054102 (2010).
[19] H. Ramezani *et al.*, Phys. Rev. A **85**, 013818 (2012)
[20] Z. Lin, *et al.*, Phys. Rev. Lett **106**, 213901 (2011).
[21] H. Ramezani *et al.*, Phys. Rev. A **82**, 043803 (2010)
[22] J. Schindler *et al.*, Phys. Rev. A **84**, 040101(R) (2011).
[23] Z. Lin *et al.*, Phys. Rev. A **85**, 050101(R) (2012)
[24] H. Ramezani *et al.*, Phys. Rev. A **85**, 062122 (2012)
[25] F. Kh. Abdullaev *et al.*, Phys. Rev. A **83**, 041805(R) (2011); A. Miroshnichenko, B. A. Malomed, Y. S. Kivshar, Phys. Rev. A **84**, 012123 (2011).
[26] M. Duanmu *et al.*, [quant-ph:1210.3871]; Y. He *et al.*, Phys. Rev. A **85**, 013831 (2012); D. A. Zezyulin, Y. V. Kartashov, V. V. Konotop, Europhys. Lett. **96**, 64003 (2011);
[27] A. Cavaglia, A. Fring, B. Bagchi, J. Phys. A: Math. Theor. **44**, 325201 (2011).
[28] `http://ngspice.sourceforge.net/`.
[29] The nonlinear harmonic balance analysis was performed in Agilent's proprietary Advanced Design System (ADS) 2011, using the Large Signal S-Parameter package.
[30] Reciprocity violations can occur in linear magnetoactive media: B. Dietz *et. al.*, Phys. Rev. Lett. **98**, 074103 (2007); H. Ramezani *et al.*, Opt. Express **20**, 26200 (2012).
[31] G. Tsironis, D. Hennig, Phys. Rep. **307**, 333 (1999).